BAMS Article

Studying Urban Climate and Air Quality in the Alps

The Innsbruck Atmospheric Observatory

Thomas Karl, Alexander Gohm, Mathias W. Rotach, Helen C. Ward, Martin Graus, Alexander Cede, Georg Wohlfahrt, Albin Hammerle, Maren Haid, Martin Tiefengraber, Christian Lamprecht, Johannes Vergeiner, Axel Kreuter, Jochen Wagner, and Michael Staudinger

ABSTRACT: The Innsbruck Atmospheric Observatory (IAO) aims to investigate atmospheric chemistry, micrometeorology, and mountain meteorology in a synergistic fashion within an urban setting. A new measurement supersite has been established in order to study processes affecting the exchange of momentum, energy, trace gases, and aerosols in an Alpine urban environment. Various long-term continuous measurements are augmented by frequent focused research campaigns with state-of-the-art instrumentation, linking different classes of data and addressing significant gaps in scientific data availability for urban environments. Current activities seek to address research objectives related to the urban heat island, trace gas emissions, the influence of foehn on air quality, and the atmospheric distribution of trace gases and aerosols in a mountainous city. We present initial results from long-term operations and first highlights from two intensive operational phases, showing that 1) the exchange of greenhouse gas emissions is dominated by anthropogenic activities and is driven by location-specific venting of street canyon air; 2) foehn events significantly perturb the photostationary state indicative for an extensive and rapid airmass exchange of the valley atmosphere; 3) the temporal distribution of pollutants is often decoupled from their emissions and primarily modulated by mountain boundary layer dynamics; 4) we can detect a large number of volatile chemical products in the urban atmosphere, which can be used to fingerprint anthropogenic emission sources; and 5) the first urban carbonyl sulfide (COS) flux measurements point toward anthropogenic emission sources.

https://doi.org/10.1175/BAMS-D-19-0270.1
Corresponding author: Thomas Karl, thomas.karl@uibk.ac.at
Supplemental material: https://doi.org/10.1175/BAMS-D-19-0270.2

In final form 12 December 2019

AFFILIATIONS: Karl, Gohm, Rotach, Ward, Graus, Haid, Tiefengraber, and Lamprecht—Department of Atmospheric and Cryospheric Sciences, University of Innsbruck, Innsbruck, Austria; **Cede**—LuftBlick, Innsbruck, Austria; **Wohlfahrt and Hammerle**—Department of Ecology, University of Innsbruck, Innsbruck, Austria; **Vergeiner and Staudinger**—Zentralanstalt für Meteorologie und Geophysik, Vienna, Austria; **Kreuter**—LuftBlick, and Division for Biomedical Physics, Medical University of Innsbruck, Innsbruck, Austria; **Wagner**—Division for Biomedical Physics, Medical University of Innsbruck, Innsbruck, Austria

More than 50% of the population currently resides in urban areas and this proportion continues to grow. The UN Department of Economic and Social Affairs projects that 68% of the world population will live in urban environments by 2050. In Europe, cities already host about 74% of the population (United Nations 2019) and are a major contributor to air pollutant and greenhouse gas emissions. Urban growth, along with socioeconomic development, leads to increases in anthropogenic emissions. In future, the atmospheric input of climate and air quality relevant gases is therefore expected to be even more concentrated in and around urban environments.

Emission inputs are often one of the most uncertain components of complex atmospheric models, and development of a robust predictive capability requires accurate data and careful evaluation of bottom-up emissions (National Academy of Sciences 2016; Blain et al. 2017). As an example, ground-based remote sensing of plumes (Bishop et al. 2010; Carslaw and Rhys-Tyler 2013) and top-down eddy covariance measurements (Lee et al. 2015; Vaughan et al. 2017; Karl et al. 2017) have demonstrated that bottom-up projections of anthropogenic emissions are still subject to considerable uncertainties.

While standard air quality monitoring across Europe, the United States, and parts of Asia is reasonably well established (e.g., European Air Quality Agency 2019), process-scale investigations of the exchange of trace gases, energy and momentum are rare. Atmospheric chemistry studies have often focused on the global and regional atmosphere, but there is a growing need to develop understanding of urban chemistry and dispersion processes occurring at smaller scales. Despite the increase in experimental activities in the field of urban micrometeorology over the last 30 years (e.g., Louka et al. 2000; Rotach et al. 2005; Vogt et al. 2005; Grimmond 2007; Barlow 2014), including some observations of trace gas and aerosol exchange measurements (e.g., Nemitz et al. 2008; Velasco et al. 2009; Langford et al. 2009; Karl et al. 2009, 2018; Rantala et al. 2016), there is still a need for robust long-term observations of turbulent exchange measurements over urban areas.

After trace gases and aerosols are emitted close to the surface they will be transported and transformed within the atmospheric boundary layer (ABL), and eventually, depending on their atmospheric lifetime, distributed locally, regionally, or globally. Estimating emissions from atmospheric columns (e.g., obtained from remote sensing) or in situ concentration measurements often requires good knowledge of the structure of the ABL and the atmospheric chemistry of reactive gases and aerosols (Barth et al. 2005; Arellano et al. 2011; Lenschow et al. 2016).

Recent observations (Zhang et al. 2016) have shown that linking concentrations to emissions in the real atmosphere is a nontrivial task due to the vertical layering of reactive gases and aerosols (Lenschow et al. 1980; Vinuesa and De Arellano 2003). Observational studies in the Alps (Rotach et al. 2017), for example, have shown a complex interplay between air density gradients, vertical mixing, and valley and slope winds, which influence the mixing ratios of trace gases and aerosols (e.g., Gohm et al. 2009).

At the city scale, the presence of large roughness elements and their thermal properties modifies the lowest part of the surface layer. The near-surface layer over an urban area is generally expected to be warmer [the well-known urban heat island (UHI) effect], and the

flow within it slower, compared to the rural surroundings (Grimmond and Oke 1999). The interaction with the boundary layer as a whole, however, can sometimes lead to (early morning) urban cooling (Theeuwes et al. 2015) or an acceleration of the flow (i.e., the "urban wind island"; e.g., Droste et al. 2018). However, the complex interactions between urban surfaces and the urban boundary layer make predicting transport and diffusion of air pollutants over urban areas a challenge (e.g., Rotach et al. 2004). At small scales ["street scale"; i.e., <100 m, according to Britter and Hanna (2003)], where individual building structures are resolved, dispersion of pollutants is largely influenced by microscale features making modeling (and understanding) highly complex.

The investigation of pollutant exchange processes (and similarly, exchange processes for energy or momentum) over urban areas therefore either needs to include measurements far enough away from the surface within the inertial sublayer (usually at least two or three average building heights away from the surface) or, alternatively, a detailed coverage of the flow and turbulence structure within the roughness sublayer. Expanding traditional surface measurements with micrometeorological and remote sensing observations can give deeper insight into the evolution of air pollutants (e.g., Darbieu et al. 2015; Banerjee et al. 2018), and significantly enhance the interpretation of surface mixing ratio measurements.

The Innsbruck Atmospheric Observatory (IAO) is an attempt to bring complex measurement setups required for atmospheric chemistry together with micro- and mesoscale observations of transport. This long-term research infrastructure also opens up new avenues for linking different classes of data (e.g., in situ vs remote sensing) and addresses significant gaps in scientific data availability in urban environments. The newly established observatory will also significantly enhance long-term climate observations of the WMO Centennial Observing station in Innsbruck operated by the Austrian National Weather Service (ZAMG) and the University of Innsbruck since 1877. This manuscript describes the scientific rationale leading to the establishment of the Innsbruck Atmospheric Observatory and its relation to successful past activities such as the Mesoscale Alpine Programme (MAP) (Bougeault et al. 2001). Further, we present initial scientific highlights from two intensive operational periods (IOP2015 and IOP2018) and an outlook to future coordinated investigations of the coupled urban-atmosphere interface.

Site characteristics

The IAO is located on the Innrain campus of the University of Innsbruck (47°15′50.5″N, 11°23′08.5″E) close to the city center of Innsbruck, the fifth-largest city in Austria with approximately 130,000 inhabitants (Statistik Austria 2019). The study period referred to in this manuscript summarizes results obtained during the first 2.5 years of full operation. An important addition was the construction of a micrometeorological tower, with the top measurement level at 42.8 m above ground. A technical description including details of the instrumentation is provided in the supplementary information.

The center of Innsbruck is characterized by a mix of modern, gothic, renaissance, and baroque architecture, typical of many western European cities that were partially rebuilt after 1945. In the city center, 5–7 story buildings are typically arranged in blocks (approximately 100 m × 100 m) around a central courtyard, which contains grass, trees, and lower buildings (Fig. 1). As has been suggested for similar European cities (Christen et al. 2009), these lower buildings are not aerodynamically important but they bring down the mean building height. Within 500 m from IAO, the mean building height is 17.3 m whereas the modal building height of about 19 m corresponds to the 5–7 story buildings, which are more important in terms of their form drag. For this reason, the displacement height, z_d, is estimated as 13.3 m (0.7 m × 19 m; e.g., Grimmond and Oke 1999). The roughness length, z_0, is 1.6 m. Footprint analysis (e.g., Fig. 1, Fig. ES1 in the online supplemental material; https://doi.org/10.1175/BAMS-D–19-0270.2)

suggests 70% of the source area lies within 500 m from the tower, where the plan area fraction of buildings is 31%, roads and paved surfaces 42%, vegetation 19%, and water 8%. The land-cover fractions vary slightly in time as atmospheric conditions alter the size and position of the source area. For easterly winds, the fraction of buildings is larger (40%) and vegetation smaller (10%) than for westerly winds (25% buildings and 15% vegetation, respectively).

The wider area around Innsbruck is home to about 300,000 people, who live along the east–west-oriented Inn Valley, which represents one of the main transport routes across Europe. Each year approximately 6 million vehicles (Eurostat 2019) pass through the eastern traffic corridor of the Inn Valley. The overall length of the Inn Valley is about 510 km. Around Innsbruck it is approximately 15 km wide (peak to peak) and surrounded by mountain ridges about 2.5 km high.

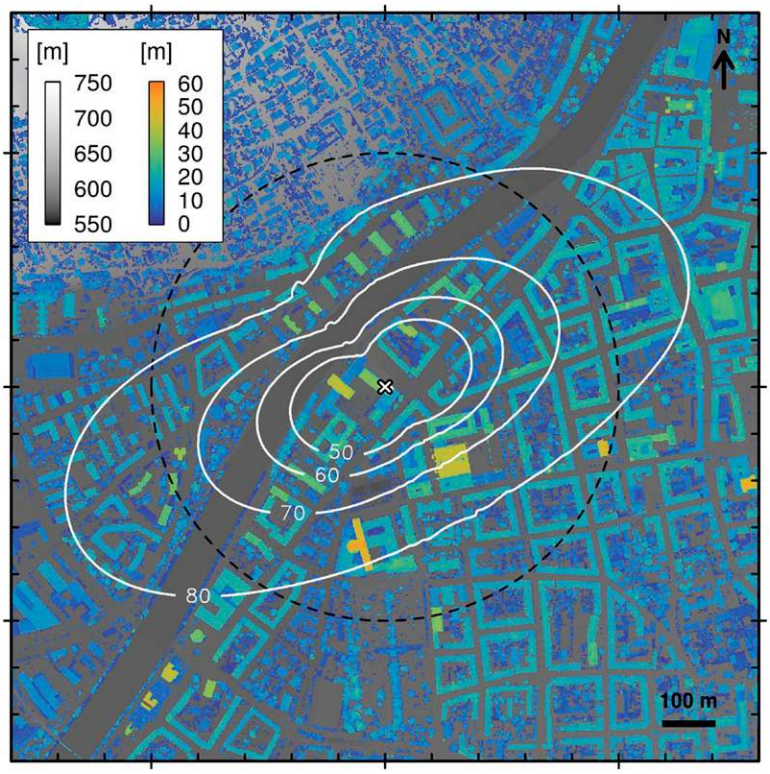

Fig. 1. 50%, 60%, 70%, and 80% composite flux source area at the IAO overlaid on ground height (gray) and building and tree height (color). The cross marks the position of the IAO tower (42.8 m above street level) and the dashed circle has a radius of 500 m. Spatial datasets are from Land Tirol. The flux footprint was calculated for 42.8 m height during the IOP2018 according to Kljun et al. (2015).

Meteorological and chemical overview

Climatology at the IAO. On a continental scale the European Alps are generally influenced by a moderately wet northwesterly flow from the Atlantic. In the northern Alps dry cold winter or warm humid summer conditions can also persist when air masses either from the eastern continent or from the Mediterranean area to the south dominate. The local climate in Innsbruck is characterized by its setting in the east–west-oriented Inn Valley, which is joined by a north–south-oriented valley (Wipp Valley) that leads to one of the major Alpine passes across the main Alpine crest. Mean monthly temperatures range from close to 0°C in winter to about 20°C in summer (Table 1).

Since the 1980s a pronounced warming trend has occurred, with the strongest warming in the last few decades in spring and summer (Zentralanstalt für Meteorologie und Geophysik 2018). Here we provide a brief overview of the climatology since the IAO was established and covering the IOP in August 2018, hereafter IOP2018. The average over the years 2016–18 shows that all months were warmer compared to the climate reference 1981–2010. Due to the topographic shielding effect the annual precipitation sum in Innsbruck is below 1,000 mm with monthly maxima in the convective season. In the central Alps precipitation shows a high year-to-year variability but no significant trend. The period 2016–18 was slightly wetter compared to the reference period. Sunshine duration sums up to around 2,000 h per year. The period 2016–18 shows an excess of about 140 h (7%) relative to the reference period, which fits well with the observed positive trend since the 1980s (Brunetti et al. 2009). Low-level temperature inversions can be a particular issue for air quality during the cold season. The inversion frequency in an approximately 340 m thick layer from the valley ground peaks in December and January, with a yearly average of 16% (Table 1).

The valley topography leads to characteristic thermally driven along-valley winds reflecting the orientation of the valley axis. The distribution of wind direction (Fig. 2) demonstrates

Table 1. Key climatological variables at the University of Innsbruck for 2016–18, the reference period 1981–2010, and the deviation to the reference indicated by Δ. For the temperature inversion frequency the slope station Hungerburg at 342 m above the valley floor was additionally used; a long-term evaluation is not available.

Parameter	Period	Jan	Feb	Mar	Apr	May	Jun	Jul	Aug	Sep	Oct	Nov	Dec	Year
Monthly mean temperature (°C)	2016–18	−0.3	2.6	6.6	11.4	15.6	19.3	20.0	20.0	15.1	10.6	5.2	0.4	10.6
	1981–2010	−1.0	0.8	5.3	9.6	14.5	17.2	19.1	18.3	14.4	9.9	3.9	-0.1	9.3
	Δ	**0.7**	**1.8**	**1.3**	**1.8**	**1.1**	**2.1**	**0.9**	**1.7**	**0.7**	**0.7**	**1.3**	**0.5**	**1.2**
Monthly mean precipitation sum (mm)	2016–18	72.7	35.0	44.7	60.3	65.3	115.7	112.7	179.0	77.7	60.7	44.0	58.7	926.3
	1981–2010	40.5	39.3	54.9	56.1	81.7	111.7	131.6	122.2	77.1	60.0	57.0	49.5	881.6
	Δ	**32.2**	**−4.3**	**−10.2**	**4.2**	**−16.4**	**4.0**	**−18.9**	**56.8**	**0.6**	**0.7**	**−13.0**	**9.2**	**44.7**
Sunshine duration (h)	2016–18	107.0	109.3	176.0	217.0	223.3	222.3	227.3	235.0	198.7	172.3	96.3	103.3	2,088.0
	1981–2010	100.0	123.0	163.0	180.0	205.0	200.0	231.0	213.0	183.0	163.0	102.0	83.0	1,946.0
	Δ	**7.0**	**−13.7**	**13.0**	**37.0**	**18.3**	**22.3**	**−3.7**	**22.0**	**15.7**	**9.3**	**−5.7**	**20.3**	**142.0**
Foehn (h)	2016–18	8.7	33.8	44.3	88.0	49.5	3.8	0.0	7.7	2.7	26.2	36.2	10.3	311.2
	1981–2010	17.5	21.7	40.8	72.9	68.0	21.8	14.5	14.7	28.6	41.5	29.5	18.1	389.5
	Δ	**−8.8**	**12.1**	**3.5**	**15.1**	**−18.5**	**−18.0**	**−14.5**	**−7.0**	**−25.9**	**−15.3**	**6.7**	**−7.8**	**−78.3**
Temperature inversion frequency (%)	2016–18	37	21	11	11	7	2	1	5	10	23	25	45	16
	1981–2010	n. a.	n. a.	n. a.	n. a.	n. a.	n. a.	n. a.	n. a.	n. a.	n. a.	n. a.	n. a.	n. a.

the channeling of the flow by the Inn Valley. The northeasterly upvalley flow tends to be stronger than the southwesterly downvalley flow. Due to Innsbruck's location north of the exit of the Wipp Valley, the strongest winds are southerly foehn winds. In the period 2016–18, about 311 h of foehn conditions per year were observed with a bimodal structure peaking in spring and autumn. In winter, foehn winds often do not reach the bottom of the valley due to a stably stratified cold pool and the summer minimum reflects rare southerly flow conditions. During the IOP2018 (Table ES3) we additionally measured winds in the street canyon [3.0 m above ground level (AGL)]. Here the orientation of the street becomes more important in channeling the flow (Fig. ES3b). At both locations (tower top and street canyon), we observed wind directional changes from downvalley (southwesterly) to upvalley (northeasterly) at about 1000 UTC, and back again after 2300 UTC.

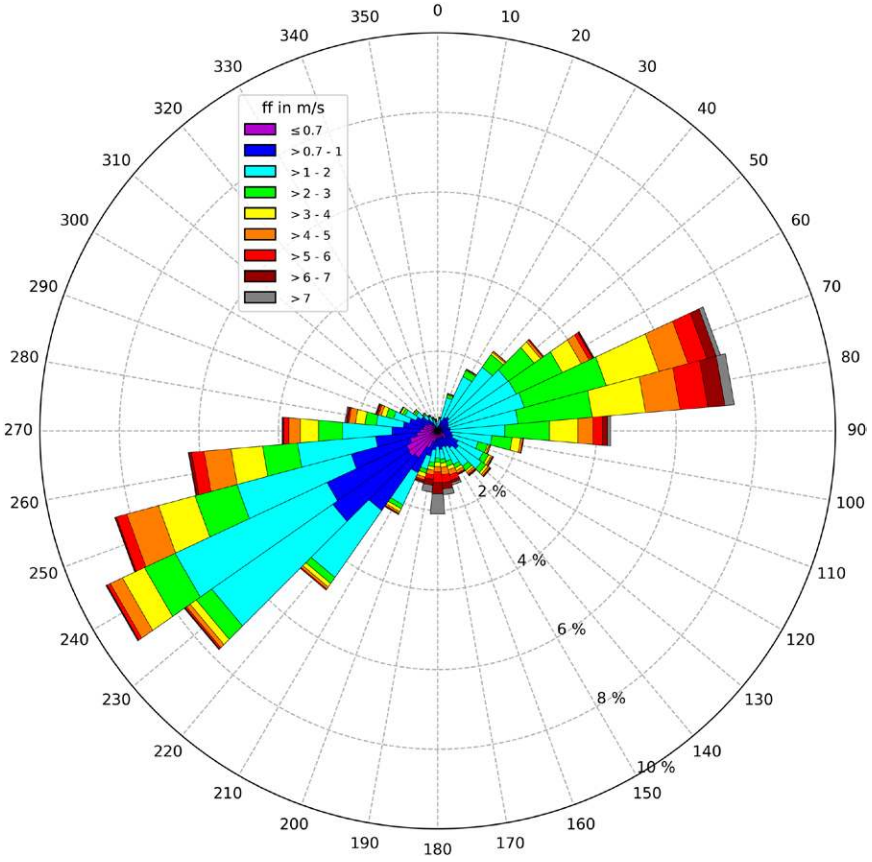

Fig. 2. Distribution of wind direction at Innsbruck University in the period 2016–18 color-coded with the wind speed frequency in each 10° wind sector. Wind rose is based on half-hourly mean values.

Micrometeorological aspects. During the IOP2018 we augmented long-term micrometeorological observations at the rooftop with measurements conducted at the street level. Due to their different locations, there are noticeable differences between fluxes measured at the rooftop and in the street canyon (Fig. 3). First, the shortwave radiation receipt ($K\downarrow$) is much lower in the street canyon due to shadowing by buildings on the southeast side of the street. The street station is only in direct sunlight during the middle of the day (0900–1430 UTC) when the elevation of the sun exceeds the height of the buildings or when the sun's azimuth lies between two buildings. During rest of the day the street canyon is shaded and the radiometer records the diffuse radiation received. This is only about 100 W m^{-2} compared to about 400–600 W m^{-2} at the tower top. On cloudy days, $K\downarrow$ is similar at both sites. Outgoing shortwave radiation ($K\uparrow$) follows a similar diurnal course to $K\downarrow$. The midday albedo on the rooftop is slightly higher (approximately 0.19) than in the street (approximately 0.14), partly due to the different materials in the field of view of the radiometer. While the tower radiometer sees mainly light-colored roof surfaces, the radiometer at the street station sees grass and dark road surfaces.

Incoming longwave radiation was higher at the street canyon level due to the larger fraction of warmer buildings as opposed to cold sky in the field of view of the upward-looking pyrgeometer. Conversely, the outgoing longwave radiation was lower at the street canyon level

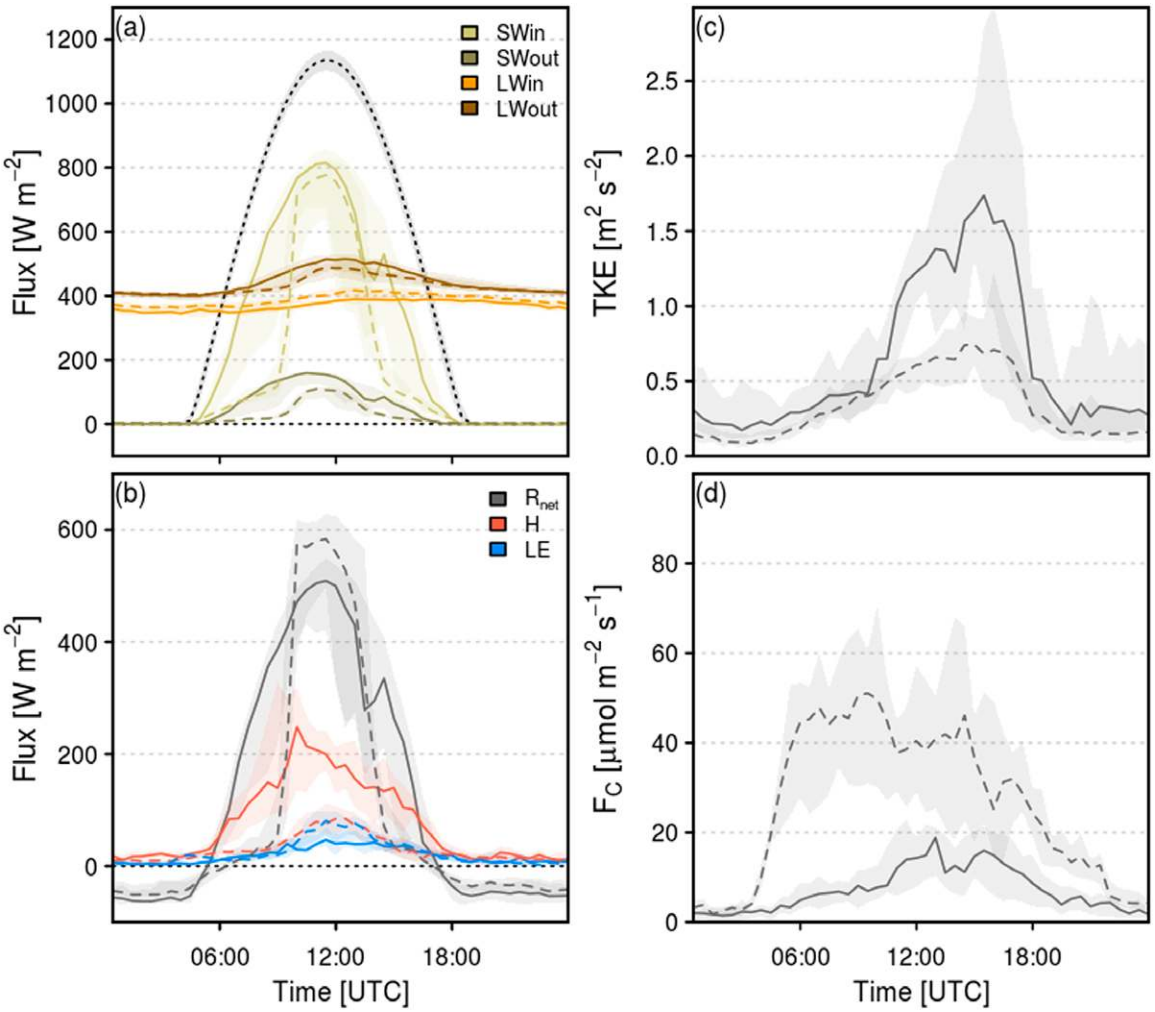

Fig. 3. Median diurnal cycles and interquartile ranges (shaded) of (a) radiative fluxes, (b) net radiation (Q^*) and turbulent sensible (H) and latent (LE) heat fluxes, (c) turbulent kinetic energy (TKE), and (d) carbon dioxide fluxes observed at the rooftop station (solid lines) and street canyon station (dashed lines) during August 2018 (IOP2018). The dotted black line in (a) indicates the incoming shortwave radiation at the top of the atmosphere.

suggesting the surfaces in the field of view of the downward-looking pyrgeometer are colder and/or characterized by lower emissivity compared to the surfaces in the field of view of the IAO net radiometer. These differences in radiation components combine to give markedly different net radiation for each site (Fig. 3b). The impact of building shading is still evident but Q^* is higher at the street station during the middle of the day due to the lower outgoing shortwave and longwave components and greater incoming longwave component.

In urban environments the available energy is supplemented by heat released by human activities (building energy use, fuel combustion for transport and human metabolism), but the main energy input in summer is from the net radiation. At the IAO tower the sensible heat flux (H) is much larger than the latent heat flux (LE), which reflects the lack of readily available moisture from largely impervious construction materials and the small proportion of vegetation in the source area. On average, 45% of the daytime net radiation is partitioned into H and only 10% into LE. The daytime Bowen ratio (H/LE) lies between about 2 and 6, which is comparable to other city-center sites with low vegetation fractions (e.g., Basel and London; Christen and Vogt 2004; Kotthaus and Grimmond 2014) The bulk of the remaining energy is stored in the urban surface. For the street station the partitioning between H and LE is more equal: H is much lower and LE is slightly higher, attributed to the greater proportion of vegetation in the source area and the limited heating of surfaces when the street is in shade.

These results highlight important issues concerning measurements in urban areas. First, to obtain representative observations for the local scale, measurements should be made above the roughness sublayer (e.g., if the street station had been installed in a larger green area or a car park, the results would be different). Second, although the turbulent fluxes are larger during the period when the street-level station receives direct solar radiation, the response of the surface is clearly not instantaneous. Third, the source area of radiation and turbulent flux measurements are very different, which should be kept in mind when analyzing data in spatially and/or temporally heterogeneous environments.

The CO_2 flux at the street station is much larger than at the tower top. This is partly due to the source area composition (the tower source area is composed of a range of surfaces of which only about 10%–15% are roads, whereas the street station is installed right next to a busy road), and partly due to the atmospheric conditions at the sites. Close to the floor of the street canyon, turbulent mixing is much smaller than at the tower top (Fig. 3c), which means that the CO_2 emissions from traffic are not easily transported away from the sensor and dispersed. Instead, the CO_2 concentration builds up near street level (e.g., Vogt et al. 2005) and the resulting large concentration gradient drives the high fluxes (Fig. 3d). CO_2 fluxes observed at the main IAO tower are always positive, indicating that the city is a clear source of CO_2 all year. Any photosynthetic uptake of CO_2 is masked by the anthropogenic emissions; however, CO_2 fluxes are smaller during the summer, which may be a combination of increased vegetation activity and reduced anthropogenic CO_2 emissions. Seasonal differences in the flux footprint (e.g., varying surface composition) possibly also play a role.

Atmospheric chemistry in urbanized valleys. The Inn Valley could be regarded as a large photochemical reactor under weak synoptic forcing. High nitrogen oxides (NO_x) emissions injected at the urbanized valley bottom mix with reactive biogenic precursors emitted along forested slopes resulting in a potentially significant haze factory. The main drivers for urban gas-phase chemistry are NO_x emissions, which are typically present in excess, as well as CO and nonmethane volatile organic compound (NMVOC) emissions. In the Inn Valley, aromatic VOCs (e.g., BTEX), CO, and aerosols ($PM_{2.5}$ and PM_{10}), have seen a trend reversal, where concentration levels have decreased considerably, despite increasing traffic volume and population growth (Umweltbundesamt Austria 2019). This can be attributed to decreasing emissions from traffic in many developed economies (McDonald et al. 2013; Ehlers et al. 2016). The fraction of

other anthropogenic NMVOC sources however is believed to have increased and might have previously been underestimated (Karl et al. 2018; McDonald et al. 2018). New observational tools allow fluxes of a wide array of NMVOCs to be quantified (see science highlight in the "Characterizing the distribution of NMVOC in Innsbruck" section).

A limited number of studies on NMVOC measurements in the Alps (e.g., Prévôt et al. 2000; Dommen et al. 2001; Holzinger et al. 2001; Schnitzhofer et al. 2008) suggest that the general distribution of sources is comparable to other areas across Europe, with the exception that anthropogenic emissions are often concentrated along valleys, and biogenic emissions dominate along alpine slopes. The mountain circulation system can redistribute biogenic and anthropogenic NMVOC effectively during summer, or inhibit the mixing of these NMVOC during stagnant wintertime temperature inversions. Nitrogen oxides are primarily emitted along valley centers, where the density of roads and population is highest. Nitrogen dioxide (NO_2), which is toxic and contributes to tropospheric ozone formation, has not exhibited a significant trend reversal, and NO_2/NO_x ratios have increased since 2000, similar to other European areas (Grange et al. 2017). It is suspected that the proliferation of the diesel fleet has led to this regional NO_2 problem, where many regions across Europe are currently challenged by excessive amounts of NO_2 (Franco et al. 2014; Carslaw et al. 2016).

Current activities at the IAO therefore also focus on urban emission sources of nitrogen oxides along with NMVOC. Direct flux measurements of NO_x and CO_2 (Karl et al. 2017) showed that urban-scale NO_x emission factors were substantially higher than some projections based on various bottom-up emission inventories used for air quality (AQ) modeling. Part of the discrepancy can likely be explained by underreported emissions from the transport sector, which has a major impact on the accuracy of European NO_x emission inventories. One major topic we seek to address on a larger scale is to understand important driving factors controlling the abundance and distribution of NO_x and O_3 within the city and the Inn Valley.

To illustrate the effects of chemistry and transport on O_3, we can for example look at the photochemical state of ozone production. The photostationary state (PSS; or Φ) of the NO–NO_2–O_3 triad is defined after Leighton (1961) as

$$\Phi = \frac{j_{NO_2}[NO_2]}{k[NO][O_3]}, \qquad (1)$$

where j_{NO_2} is the photolysis rate of NO_2; [NO_2], [NO], and [O_3] represent the concentrations of NO, NO_2, and O_3, respectively; and k is the reaction rate constant between the reaction of NO with O_3.

The PSS (i.e., Φ) represents the steady-state solution of the fast null cycle reactions of the NO–NO_2–O_3 triad. Within the reactions between NO, NO_2, and O_3 these species are interconverted but not lost due to oxidation. If an unperturbed steady state is achieved, Φ should therefore be one. In urban areas where NO levels are high, O_3 is efficiently converted to NO_2 by reaction with NO, and NO_2 serves as a temporary reservoir of O_x (:= O_3 + NO_2). The cycling between NO, NO_2, and O_3 under these conditions is fast, and PSS is typically achieved within 100 s. When NO_x concentrations during daytime are high the PSS often exhibits ratios close to 1 (i.e., photostationary state is achieved). PSS deviations greater than one have been attributed to additional chemistry (e.g., via HO_2 or RO_2 + NO reactions) (e.g., Carpenter et al. 1998; Mannschreck et al. 2004; Griffin et al. 2007) or transport phenomena (e.g., De Arellano et al. 1993; Khalil 2018) On the other hand deviations below 1 can only be explained by transport processes of precursors. Thus the analysis of PSS allows to disentangle the net import of ozone from local conversion processes.

Close to IAO there are three AQ stations, that allow measurements conducted at the IAO to be extended spatially and temporally. Figure 4 shows a merged analysis based on measurements conducted at an AQ site (EU AT72106, located within about 500 m of the IAO) for foehn and nonfoehn days in 2015. NO, NO_2, and O_3 were measured at the AQ site, photolysis

rates and temperature were calculated from data obtained at the IAO. PSS on nonfoehn days is on average close to one (i.e., $\Phi = 1$), comparable to many urban areas. We clearly see this effect during foehn events, where Φ drops significantly below 1, suggesting that a substantial amount of ozone is imported into the valley during these events. For example, a PSS of 0.5 ($\Phi = 0.5$; Fig. 4) indicates that 50% of ozone is imported into the valley during foehn events. Figure 4 also shows that the distribution of PSS on foehn days is significantly skewed due to a complex interplay between local precursor emissions, chemistry, and airmass advection. Ozone transport phenomena in Alpine valleys during foehn events have been investigated in the past. For example, Seibert et al. (2000) summarized processes leading to ozone enhancement during foehn events. It should be noted that the interconversion between NO, NO_2, and O_3 does not lead to a net loss of NO_x and that the atmospheric lifetime of NO_x is primarily driven by oxidation of NO_2 with OH. Recently, Laughner and Cohen (2019) detected a change of NO_x lifetime in North American cities due to changing emissions. Based on their assessment, we estimate a NO_x lifetime of 6–7 h for Innsbruck (e.g., NO_2 column: 1.3×10^{16} molecules cm^{-3}; OH reactivity: 10–15 s^{-1}), which is at the upper limit compared to U.S. cities.

Two Pandora spectrometer systems [details provided in the online supplemental material (https://doi.org/10.1175/BAMS-D–19-0270.2)] measure long-term column densities of NO_2 and O_3 at the IAO. The combination of long-term Pandora observations at the IAO, with globally derived remote sensing products (e.g., Sentinel-5b) and in situ datasets (at the IAO and nearby AQ stations) will allow studies spanning different spatial scales across the Inn Valley. The Pandora data for NO_2 and O_3 are now routinely processed and provided through the Pandonia Global Network.

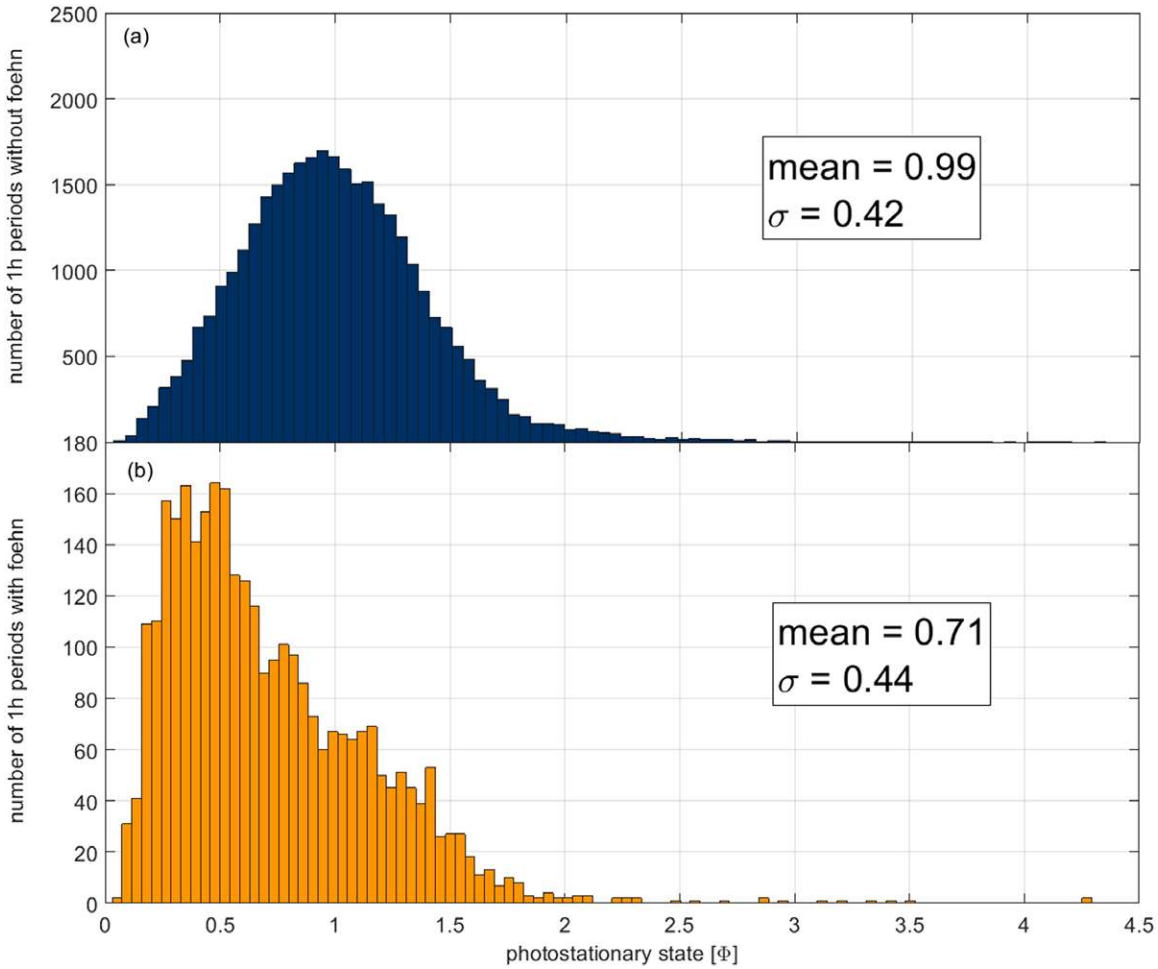

Fig. 4. Distribution (i.e., number of hourly data) of daytime photostationary state (Φ) observed in Innsbruck for (a) nonfoehn and (b) foehn days during 2015.

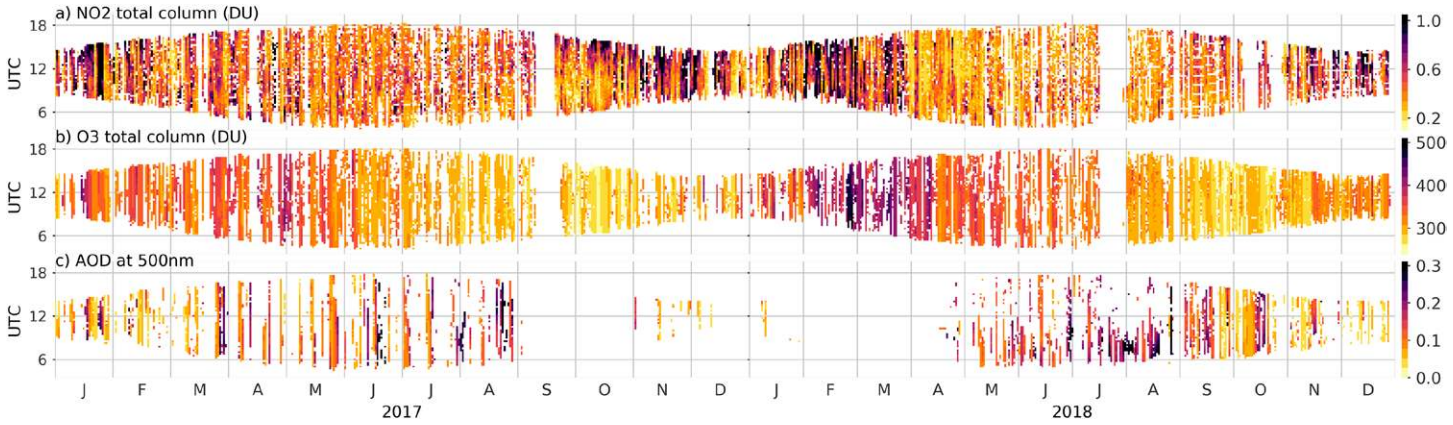

Fig. 5. Pandora and sun-photometer column measurements from 1 Jan 2017 to 31 Dec 2018: (a) NO_2 total columns (Pandora), (b) O_3 total columns (Pandora), and (c) aerosol optical depth (AOD) at 500 nm (sun photometer). Only measurements of highest data quality are shown (i.e., measurements contaminated by clouds are filtered). For visualization purposes, datasets are grouped to 15 min bins (the data gap for AOD beginning 2018 was due to instrument recalibration).

Aerosol optical depth (AOD) can be additionally obtained from a four channel sun photometer. As an example, NO_2, AOD, and O_3 column data for an aggregated time series between 2017 and 2018 for Innsbruck are shown in Figs. 5a–c. These data reflect the path-integrated valley atmosphere. As can be seen, NO_2 columns are highest during the wintertime when strong low-level temperature inversions and associated reduced mixing lead to an accumulation of air pollutants within the valley. UV/visible remote sensing techniques typically obtain NO_2 rather than NO_x, and NO_x trends have often been estimated inferentially in the past (Reuter et al. 2014). For Innsbruck, our goal is to expand the trend analysis regarding valley integrated NO_x concentrations based on a combination of remote sensing, modeling and in situ observations.

Further, the Pandora remote sensing instruments also serve as a testbed for the Pandonia Global Network. New developments in instrument operation software, data acquisition software, observation modes, measurement techniques, optics, and other hardware are first introduced at IAO and then, after successful testing, applied to all instruments in the network. Usually the changes are introduced in one of the two instruments and the other one is used as a reference. For some developments the unique geographical situation of Innsbruck has been utilized. For example, one of the instruments was temporarily moved to a high altitude site (Hafelekar, horizontal distance from IAO 4.5 km, vertical distance 1.6 km) in order to validate tropospheric column retrievals.

First research insights

To illustrate the suite of available observations this section presents three additional highlights from two IOPs (IOP2015 and IOP2018; Table ES3), when a significant portion of continuous and campaign-based instrumentation was operational.

A day in the valley: Combined remote sensing and in situ measurements during the European heat wave in 2018. By combining various remote sensing and in situ datasets, the impact of boundary layer evolution on fluxes and concentrations of trace gases can be analyzed. As an example we show data from one representative day (28 August 2018) toward the end of the 2018 heat wave. This day was characterized by weak synoptic forcing and clear-sky conditions resulting in a strong diurnal cycle of radiative forcing (Fig. 6d) favoring the generation of thermally driven flows in the Inn Valley (Figs. 6a,c) with downvalley (westerly) winds during nighttime and upvalley (easterly) winds during daytime (e.g., Vergeiner and Dreiseitl 1987; Zängl 2004; Goger et al. 2018; Lehner et al. 2019). The morning transition from downvalley to upvalley flow occurred at about 1000 UTC (cf. “Climatology at the IAO”

section). The daytime heating led to a continuous growth of the convective boundary layer during the morning, as illustrated by the evolution of the pseudovertical profile of potential temperature measured by weather stations along the mountain slope north of Innsbruck (Fig. 6a). The boundary layer height deduced from the vertical velocity variance retrieved from

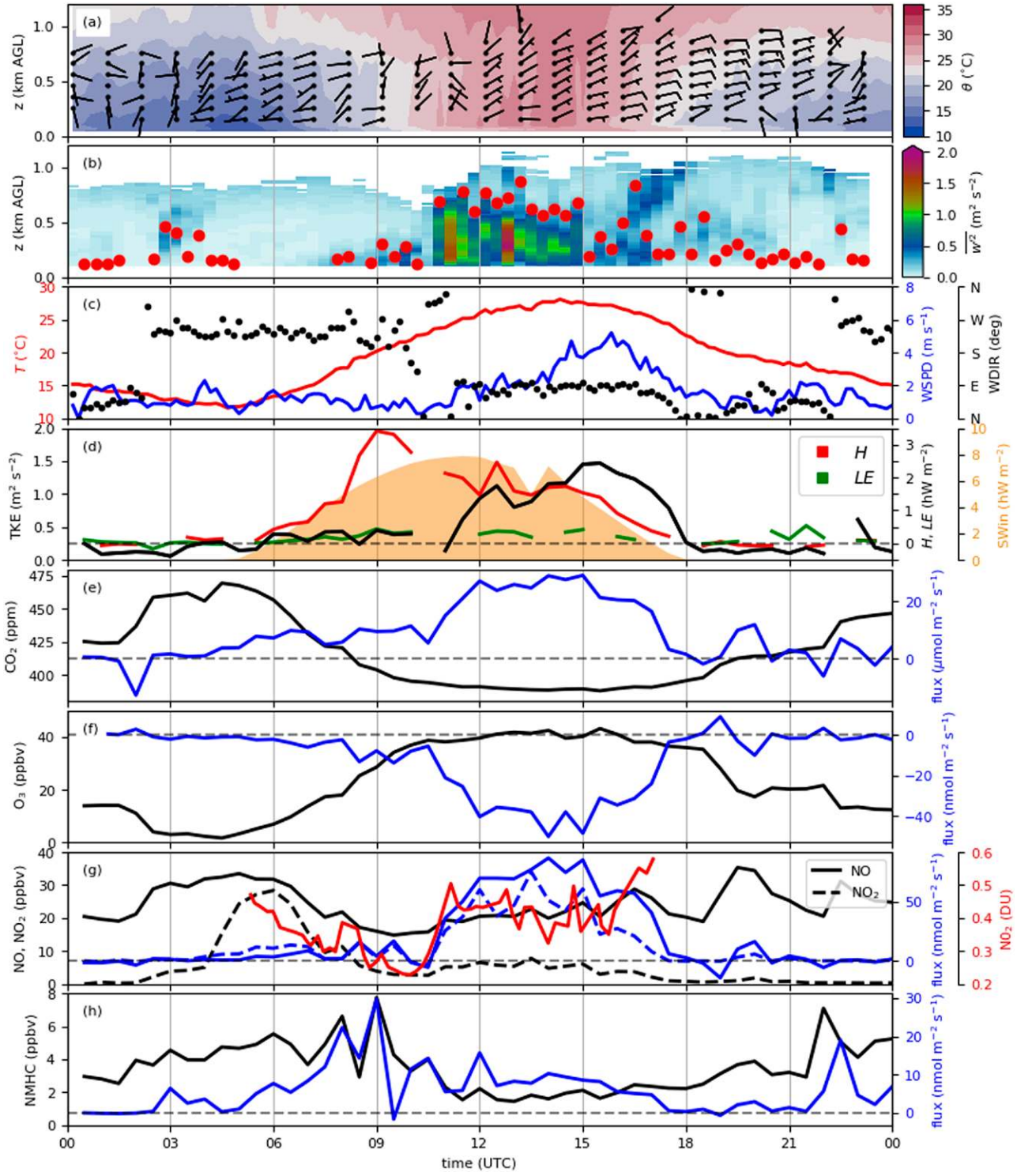

Fig. 6. Measurements on 28 Aug 2018: (a) Potential temperature (color contours) and wind barbs for horizontal winds as a function of height, (b) vertical velocity variance (color contours) and corresponding ABL height (red dots), (c) near-surface temperature (red), wind speed (blue), and wind direction (black), (d) TKE (black), sensible and latent heat fluxes (red and green), and shortwave incoming radiation (orange), (e) CO_2 fluxes (blue) and mixing ratios (black), (f) ozone fluxes (blue) and mixing ratios (black), (g) NO and NO_2 fluxes (blue solid and dashed), NO and NO_2 mixing ratios (black solid and dashed), and NO_2 columns (red), and (h) summed NMHC concentrations (black) and fluxes (blue).

a Doppler wind lidar peaked at midday between about 600 and 900 m AGL (Fig. 6b). Late afternoon (e.g., 16 h) when the vertical velocity variance rapidly decreases for some period, the estimated ABL retrieved from the wind lidar seems biased low. More research is needed to investigate the sensitivity of ABL retrievals under these conditions. Sensible heat peaked in the morning and, as expected from the land-cover characteristics ("Site characteristics" section), latent heat fluxes were low (Fig. 6d).

Urban trace gases fluxes (CO_2, NMHC, NO_x, and O_3) peaked during midday (Figs. 6e–h), along with turbulent kinetic energy (TKE) (Fig. 6d). NO_x has strong emission sources along the valley, suppressing net ozone formation in the urban core. Ozone exhibited a substantial downward flux above the city (Fig. 6f), which is mainly driven by the conversion of NO to NO_2. With the exception of ozone, which is primarily photochemically produced, all other trace gases exhibit concentration minima during daytime (Figs. 6d–h) due to dilution initiated by ABL growth and thermally driven slope and valley winds.

We also show the diurnal evolution of ground-based NO_2 column data obtained by the Pandora system (Fig. 6g). The interpretation of the diurnal cycle is more complex compared to in situ measurements near the ground. While all NO_x concentration data (in situ and column) exhibit a morning peak, their interpretation might differ. In situ NO_2 shows an early morning peak, which is caused by increasing NO_x emissions due to traffic and a shallow ABL height. NO rapidly reacts with O_3, so that a large fraction of NO_x is converted to NO_2 suppressing local ozone concentrations. The decline of in situ NO_2 mixing ratios is caused by dilution due to ABL growth. The latter alone however cannot explain the decline of column NO_2, since this quantity should be invariant to vertical dilution effects. However, as the sun moves from east to west, the Pandora column measurement will scan different parts of the Inn Valley. At about 0500 UTC the sun elevation angle was 5°, and the azimuth of the Pandora observations pointed east. This is an area of increased NO_x pollution sources due to the A12 motorway. Declining NO_2 column densities until about 1000 UTC likely reflect the fact that the system measured less polluted air masses toward the south of Innsbruck, which is still characterized by relatively clean downvalley flow. At the time when the valley wind system transitions from a westerly to an easterly flow, the increase in NO_2 column density likely reflects the fact that more polluted air masses were advected past the field of view of the Pandora instrument, which at this time was facing south.

Fluxes and concentrations of nonmethane hydrocarbons (NMHC) are generally characterized by an increase during the rush hour (Fig. 6h). Here we only show the sum of detected hydrocarbons (i.e., C_xH_y), which by definition always exhibit an emission flux, because they are only released by primary emission sources (e.g., no photochemical production). NMHC were measured by an online technique [proton-transfer-reaction quadrupole-interface time-of-flight mass spectrometer (PTR-QiTOFMS)]. Since certain classes of NMHC (e.g., lightweight alkanes) are not detected by this measurement method, the plotted total concentration represents a lower limit, although we have previously shown that the diurnal cycle is quite representative of the bulk anthropogenic NMHC flux (Karl et al. 2018). Following the increase during rush hour NMHC concentrations generally decrease due to dilution, similar to other trace gases (e.g., CO_2, NO_x). NMHC fluxes stabilize during daytime largely following the diurnal course of CO_2 fluxes. Emissions of urban NMHC, and more generally NMVOC, are quite complex owing to many different anthropogenic emission sources (McDonald et al. 2018; Karl et al. 2018). Certain NMVOC can be used as specific tracers to provide chemical fingerprints. The next section discusses an example of NMVOC observations at the IAO in more detail.

Characterizing the distribution of NMVOC in Innsbruck. A major atmospheric chemistry focus concerns the complexity of nonmethane organic compound (NMVOC) emissions and distributions, which fuel ozone chemistry and serve as precursors to secondary organic

aerosol formation (Jenkin et al. 1997; Jimenez et al. 2009). Based on PTR-MS technology we have conducted a series of studies on the exchange of urban NMVOC and were able to show that urban emission sources are diverse and can exhibit complex emission patterns (Karl et al. 2018). The distribution of urban NMVOCs is nowadays mostly dominated by volatile chemical products. Some of these NMVOC emission fluxes can serve as unique markers. For example, we have detected trace amounts of evaporative emissions from cosmetic products that can serve as urban human markers (Fig. 7). Figure 7 shows the sum of D3, D4, D5, and D6 siloxane fluxes measured at the IAO. Emission fluxes of these compounds exhibit a significant rush hour peak, and show pronounced differences between weekdays and Sundays.

More established markers include acetonitrile or furans that are indicative of burning activities (e.g., Coggon et al. 2016). Other tracers are biogenic VOCs (trees), and combustion and fuel evaporative NMVOC, such as aromatic species (e.g., benzene and toluene). NMVOC at the IAO are measured using a PTR-QiTOFMS instrument, which allows 10 Hz acquisitions of about 300,000 mass channels, enabling a wide range of NMVOCs to be scanned. Strictly speaking, the instrument enables the 10 Hz online measurement of the isobaric composition of the NMVOC pool. The selectivity of these types of measurements for atmospheric chemistry–related research has been evaluated over the past 20 years (e.g., Lindinger and Jordan 1998; De Gouw et al. 2003; Graus et al. 2010; Karl et al. 2012; Sulzer et al. 2013).

A useful quantity to normalize the impact of reactive carbon (e.g., NMVOC) on local radical (and ozone) chemistry is the OH reactivity, which is defined as

$$R_{\mathrm{OH}} = \sum_i k_{\mathrm{OH}}(i)[\mathrm{NMVOC}_i], \qquad (2)$$

where $k_{\mathrm{OH}}(i)$ represents the OH rate constant for the ith NMVOC species, and $[\mathrm{NVMOC}]_i$ is the atmospheric concentration of the ith NMVOC. The OH reactivity is inversely proportional to the OH lifetime. For example, an OH reactivity of 10 s^{-1} corresponds to an OH lifetime of 0.1 s. Due to the extremely short lifetime OH is therefore not transported in the atmosphere and results from the local chemical balance of OH production and destruction. The OH reactivity is a very useful measure to constrain the catalytic ozone production efficiency in an air mass. The OH reactivity R_{OH} divided by the chemical loss of NO_2 (i.e., reaction of NO_2 with OH) is defined as the chain length for ozone production. A chain length of 10 would, for example, mean that 10 molecules of ozone are produced before 1 NO_2 is being oxidized.

Measuring OH reactivity of the individual pool of NMVOC is still difficult and often limited by analytical techniques. Systems that can indirectly infer the overall OH reactivity (e.g., Sinha et al. 2012; Dolgorouky et al. 2012; Brune et al. 2016) have suggested missing sources of NMVOCs in various environments. Bottom-up-scaling approaches of NMVOC reactivity, by definition, always represent a lower limit, because some species are hard to analytically identify or sample. In case of

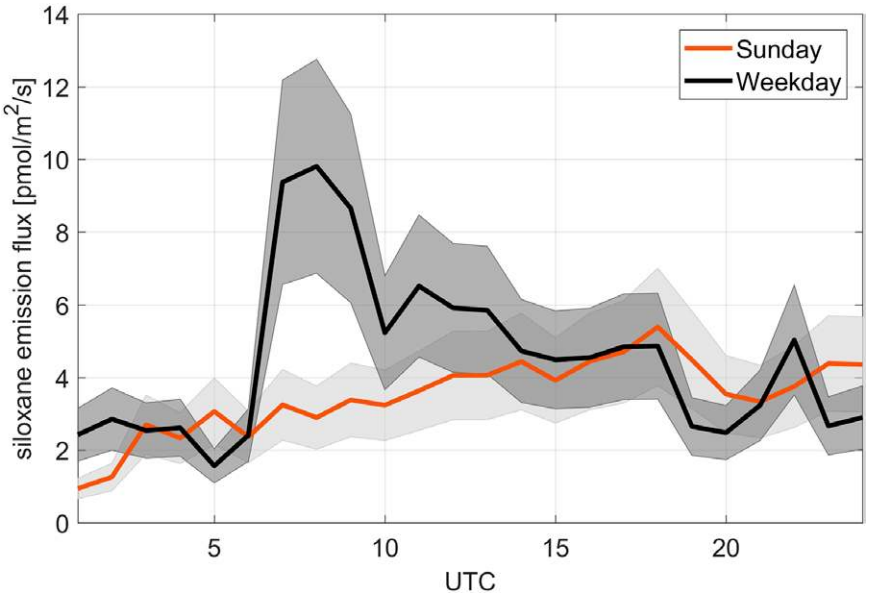

Fig. 7. Diurnal variation (median and standard deviation) of siloxane fluxes on weekdays (i.e., Tuesday–Thursday) and Sunday during the IOP2015.

PTR-TOF-MS measurements, the mass spectrometric assignment to a specific isomer is also not always possible. However, in order to get a first glimpse at the measured urban NMVOC reactivity in Innsbruck, we performed the following data mining experiment: based on measurements conducted during the summer of 2015 (Karl et al. 2018), we extracted daily concentrations of the entire mass spectrum from a PTR-TOF-MS instrument, which included 163 isobaric species up to m/z 445 (Table ES3). Next, the 10 most common isomeric molecular species were extracted from chemical databases and structurally assigned to the isobaric species list (National Institute for Standards 2018; Chemspider 2018) For each of the potentially 1,630 species an OH rate constant (US EPA 2017) was determined. Theoretically this leads to 10^{163} possible realizations of OH reactivity. For compounds that could be uniquely assigned, only one species was used for the analysis (e.g., methanol), for some other species the list was constrained to the most relevant atmospheric species (a full table is provided in the supplementary information).

Finally, this led to a refined list of 1,436 species. To make the problem tractable one million random subsamples of this list were created and used to calculate a statistical distribution of OH reactivity. The resulting distribution is shown in Fig. 8 suggesting a most likely OH reactivity bound between 10.0 and 12.5 s^{-1} (median = 10.9 ± 1.4 s^{-1}). This number likely represents somewhat of a lower limit since some lightweight hydrocarbons (C2–C4 species) are not quantitatively detected by PTR technology. Based on literature reports (Hellen 2003; Dolgorouky et al. 2012; Borbon et al. 2013) these compounds missing from the current analysis would typically add another 0.7–2 s^{-1} in European cities. For comparison, an average campaign OH reactivity of 20 s^{-1} has been reported during the field-intensive [Megacities: Emissions, urban, regional and Global Atmospheric Pollution and climate effects, and Integrated tools for assessment and mitigation (MEGAPOLI)] for Paris (Dolgorouky et al. 2012). During MEGAPOLI a large fraction of oxygenated VOCs was not measured, which could be attributed to a missing urban NMVOC reactivity. Indeed if we scale OH reactivity in both cities to the measured benzene reactivity, and compare these measurements, the analysis for Innsbruck would suggest a value that is about 1.5 times higher, and could explain some of the missing OH reactivity inferred from indirect methods in Paris. This preliminary analysis warrants future investigations about the cycling of NMVOC and organic carbon in the urban atmosphere, and the role of biogenic and oxidized NMVOCs in Alpine regions. Combining different measurement techniques and top-down observations of OH reactivity could help tackle this problem, and determine important sources of NMVOC in urban environments.

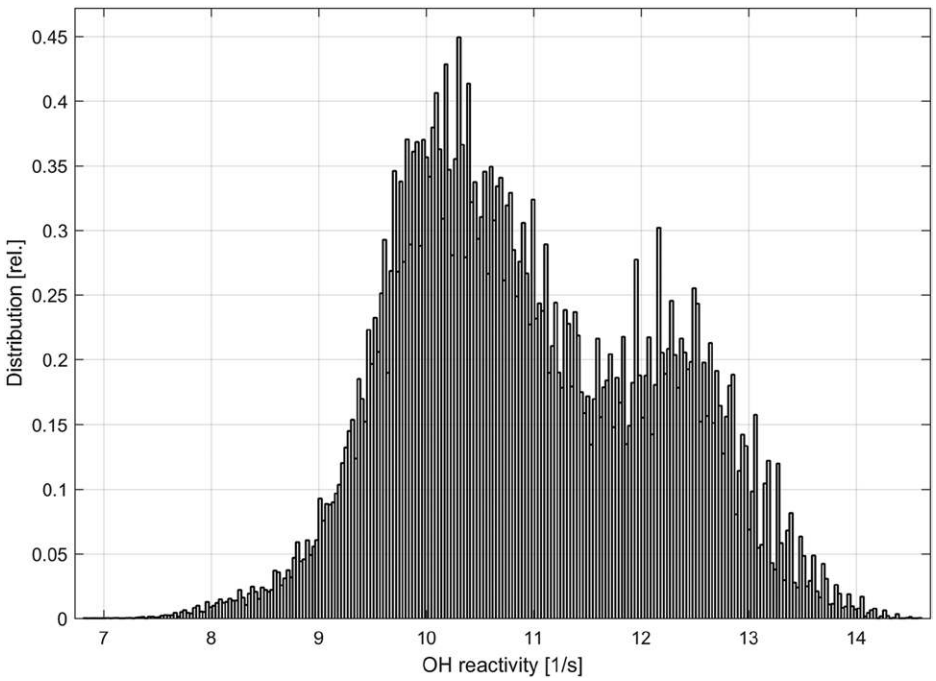

Fig. 8. Relative distribution of the estimated OH reactivity for Innsbruck during the IOP2015 based on data initially published by Karl et al. (2018).

The issue of NMVOC loading also has ramifications for understanding the distribution of aerosols. For example, it has been recently postulated that monoterpenes act as

the single biggest summertime source for secondary aerosols in the southeastern United States (Zhang et al. 2018). A high aerosol forming potential from monoterpenes has also been confirmed by numerous laboratory studies (e.g., Stolzenburg et al. 2018; Berndt et al. 2018; Gkatzelis et al. 2018). Since European ecosystems tend to emit a larger fraction of assimilated carbon in form of monoterpenes rather than isoprene when compared to their American counterparts (Simpson et al. 1999; Schnitzler et al. 2002; Calfapietra et al. 2013; Llusia et al. 2013), the fraction of biogenically derived aerosol could be particularly large in the Alps, where they are mixed into an NO_x rich valley atmosphere. Further study of the atmospheric chemistry in Alpine valleys (e.g., Schroeder et al. 2013) is however required to elucidate the complex behavior of secondary air pollutant formation, particularly aerosols (e.g., Aksoyoglu et al. 2014; Hodzic et al. 2016).

First urban eddy covariance fluxes of COS. Direct flux measurements of carbonyl sulfide (COS) are increasingly used to decipher photosynthetic CO_2 uptake and respiration fluxes above ecosystems. On a global scale COS is mainly produced in the oceans, and to a smaller degree by industrial activities. The uptake is dominated by plants in a fashion similar to CO_2, but in contrast to CO_2, COS is generally not emitted by plants (Whelan et al. 2018). The uptake of COS thus correlates with the photosynthetic uptake of CO_2 by plants, and thus potentially allows the photosynthetic uptake to be disentangled from the respiratory release of CO_2 in terrestrial ecosystems (Asaf et al. 2013; Spielmann et al. 2019). At the IAO we explored the possibility to use COS to identify photosynthetic uptake, since any uptake signal in the observed CO_2 fluxes would be masked by the considerable CO_2 emissions from fossil fuel combustion. During the IOP2018 we measured the flux of COS between the urban canopy and the atmosphere using a

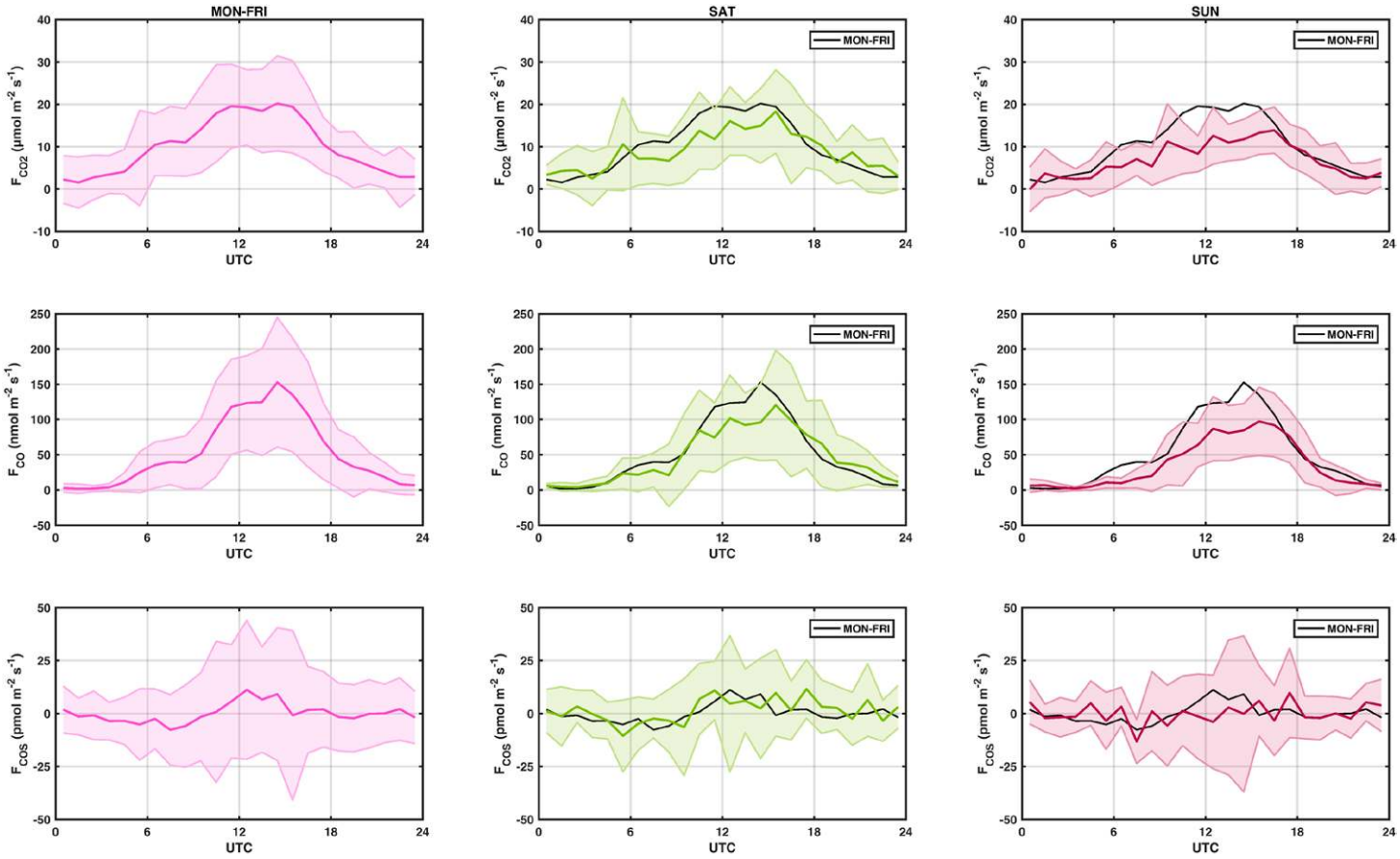

Fig. 9. Diurnal variation (mean and one standard deviation) of (top) CO_2, (middle) CO, and (bottom) COS fluxes measured above the city of Innsbruck. Data are stratified by working days (Monday–Friday), Saturdays, and Sundays (including public holidays). As reference the Monday–Friday average fluxes are also plotted in the other panels.

quantum cascade laser absorption spectrometer (MiniQCL, Aerodyne, United States) (Stimler et al. 2010).

Figure 9 shows the diurnal course of COS, CO_2, and CO fluxes for the first three weeks of IOP2018. CO fluxes are used as a surrogate for emissions from combustion sources. Generally, the COS flux was close to zero from late afternoon until after midnight, and then started to decrease slightly (i.e., net uptake of COS) until midmorning, before it changed sign around midday (i.e., net emission of COS). Net nighttime uptake of COS, when photosynthesis is halted due to the lack of sunlight, is currently understood to reflect the fact that plants do not completely close stomata in darkness, allowing COS to enter plant leaves where it is then consumed by the corresponding light-independent enzyme (Kooijmans et al. 2017). The increase in COS uptake during the early morning can then be interpreted as further opening of the stomata in order to more effectively take up CO_2, as is typically observed with terrestrial ecosystems (e.g., Spielmann et al. 2019). The subsequent switch in sign (i.e., COS being emitted from the urban canopy) reflects net sources in an urban environment.

Plant emissions of COS have only been reported for bryophytes under drying/wetting cycles (Gimeno et al. 2017) or vascular plants that received excessive amounts of sulfur fertilizer or were infected by fungi (Bloem et al. 2012). Bryophytes are thought to play a minor role in the footprint of the IAO flux measurements, while little is known regarding the sulfur metabolism and fungal infections of the vegetation in the footprint. Soils may emit COS, in particular when exposed to sunlight (Kitz et al. 2017). The major known anthropogenic COS sources that play a role in the footprint of the IAO stem from automobile exhaust emissions and the wear of automotive tires (Fried et al. 1992; Lee and Brimblecombe 2016; Zumkehr et al. 2018). Compared to working days, hardly any COS fluxes were observed on Sundays and public holidays, suggesting that vehicular COS emissions may be the major underlying source of the observed midday emission peak. Fried et al. (1992) reported vehicular COS emissions of 5.8×10^{-6} gCOS per gCO for gasoline and 2.0×10^{-4} gCOS per gCO for diesel cars. For comparison, the weekday COS per CO mass flux ratio measured at the IAO corresponds to about 2.8×10^{-4} gCOS per gCO ($R^2 = 0.45$). The correlation between COS and CO fluxes on Sundays was very poor ($R^2 = 0.01$) with a net COS flux close to zero. These measurements indicate that vehicular exhaust might be a major COS source in urban areas. Using COS as a tracer for plant photosynthesis in urban areas therefore requires an accurate characterization of these urban emission sources.

Further perspective

The European Alps are home to about 14 million inhabitants. In many parts only about 30% of the land is habitable, leading to population densities clustering along valleys that are comparable to large metropolitan agglomerations (Onida 2019). In addition, being at the crossroads between northern and southern Europe, the Alps have experienced a significant increase of goods traffic within the European Common Market, leading to an additional burden of air pollutant emissions. Particular meteorological conditions associated with complex orography can impede the dilution of air pollutants, making the region more vulnerable to air pollution episodes. Furthermore, the Alps have experienced a warming trend that is about twice as fast as the global average (Gobiet et al. 2014), and increased summer temperatures in combination with the urban heat island effect is expected to impact the quality of living in many parts (e.g., Tan et al. 2009; Sailor 2014). There is concern that climate change could further increase the burden of illness and mortality due to conditions more conducive to air pollution episodes (e.g., during heat waves).

The greening of cities has been proposed as a measure to mitigate the detrimental effects of increasing temperature and urban pollutants. However, while the cooling effect near vegetation due to evapotranspiration is well established, biogenic–anthropogenic emission

interactions are more complex, and might be particularly prominent in Alpine valleys. Thus, understanding the interplay between strong anthropogenic emission sources along urban centers in Alpine valleys, significant biogenic emissions on valley slopes, and the valley circulation connecting these is a prerequisite to develop appropriate adaptation strategies.

IAO activities aim to provide long-term observations and infrastructure to study air pollution and climate change and their interaction in an Alpine urban environment. Past intensive campaigns focused on a better understanding of gas-phase chemistry precursor emissions (e.g., Karl et al. 2017, 2018), and the influence of particular meteorological phenomena (e.g., foehn) on the transport of pollutants (Schnitzhofer et al. 2009; Gohm et al. 2009). Future plans will include more detailed investigations of the fate of pollutants including sources and transformations of aerosols and gases. The rich dataset of meteorological drivers will also spark investigations using high-resolution numerical models, capable of simulating dispersion mechanisms over complex terrain, and extend an existing Alpine network of turbulence observations (Rotach et al. 2017) to an urban site.

From an experimental point of view the IAO offers infrastructure for campaign-based community experiments providing a critical mass of core chemical and physical measurements. A special focus herein lies in the ability to provide eddy covariance observations for a wide range of chemical species, allowing the extension of traditional micrometeorological concepts to reactive gases and aerosols that participate in atmospheric chemistry. We anticipate that the infrastructure provided at the IAO can also help to test new instrumentation for micrometeorological applications taking advantage of a well-established flux tower. For long-term observations we envision tracking the evolution of important urban air pollutants (e.g., NO_x, CO_2) by directly measuring their turbulent fluxes into the atmosphere.

Acknowledgments. This work was primarily funded by the Hochschulraum-Strukturmittel (HRSM) funds sponsored by the Austrian Federal Ministry of Education, Science and Research (www.bmbwf.gv.at/), the EC Seventh Framework Program (Marie Curie Reintegration Program, "ALP-AIR," Grant 334084), and partly by the Austrian National Science Fund (FWF) Grants P30600, P29746, P26931 and P27176, and the FWF Lise Meitner Programme (M2244-N32).

References

Aksoyoglu, S., J. Keller, G. Ciarelli, A. S. H. Prévôt, and U. Baltensperger, 2014: A model study on changes of European and Swiss particulate matter, ozone and nitrogen deposition between 1990 and 2020 due to the revised Gothenburg protocol. *Atmos. Chem. Phys.*, **14**, 13 081–13 095, https://doi.org/10.5194/acp-14-13081-2014.

Arellano, J. V.-G., E. G. Patton, T. Karl, K. Van Den Dries, M. C. Barth, and J. J. Orlando, 2011: The role of boundary layer dynamics on the diurnal evolution of isoprene and the hydroxyl radical over tropical forests. *J. Geophys. Res.*, **116**, D07304, https://doi.org/10.1029/2010JD014857.

Asaf, D., E. Rotenberg, F. Tatarinov, U. Dicken, S. A. Montzka, and D. Yakir, 2013: Ecosystem photosynthesis inferred from measurements of carbonyl sulphide flux. *Nat. Geosci.*, **6**, 186–190, https://doi.org/10.1038/ngeo1730.

Banerjee, T., P. Brugger, F. De Roo, K. Kroeniger, D. Yakir, E. Rotenberg, and M. Mauder, 2018: Turbulent transport of energy across a forest and a semiarid shrubland. *Atmos. Chem. Phys.*, **18**, 10 025–10 038, https://doi.org/10.5194/acp-18-10025-2018.

Barlow, J. F., 2014: Progress in observing and modelling the urban boundary layer. *Urban Climate*, **10**, 216–240, https://doi.org/10.1016/j.uclim.2014.03.011.

Barth, M., and Coauthors, 2005: Coupling between land ecosystems and the atmospheric hydrologic cycle through biogenic aerosol pathways. *Bull. Amer. Meteor. Soc.*, **86**, 1738–1742, https://doi.org/10.1175/BAMS-86-12-1733.

Berndt, T., B. Mentler, W. Scholz, L. Fischer, H. Herrmann, M. Kulmala, and A. Hansel, 2018: Accretion product formation from ozonolysis and OH radical reaction of α-pinene: Mechanistic insight and the influence of isoprene and ethylene. *Environ. Sci. Technol.*, **52**, 11 069–11 077, https://doi.org/10.1021/acs.est.8b02210.

Bishop, G. A., A. M. Peddle, D. H. Stedman, and T. Zhan, 2010: On-road emission measurements of reactive nitrogen compounds from three California cities. *Environ. Sci. Technol.*, **44**, 3616–3620, https://doi.org/10.1021/es903722p.

Blain, D., and Coauthors, Eds., 2017: Short lived climate forcers. Institute for Global Environmental Strategies Rep., 66 pp.

Bloem, E., S. Haneklaus, J. Kesselmeier, and E. Schnug, 2012: Sulfur fertilization and fungal infections affect the exchange of H_2S and COS from agricultural crops. *J. Agric. Food Chem.*, **60**, 7588–7596, https://doi.org/10.1021/jf301912h.

Borbon, A., and Coauthors, 2013: Emission ratios of anthropogenic volatile organic compounds in northern mid-latitude megacities: Observations versus emission inventories in Los Angeles and Paris. *J. Geophys. Res. Atmos.*, **118**, 2041–2057, https://doi.org/10.1002/JGRD.50059.

Bougeault, P., and Coauthors, 2001: The MAP special observing period. *Bull. Amer. Meteor. Soc.*, **82**, 433–462, https://doi.org/10.1175/1520-0477(2001)082<0433:TMSOP>2.3.CO;2.

Britter, R. E., and S. R. Hanna, 2003: Flow and dispersion in urban areas. *Annu. Rev. Fluid Mech.*, **35**, 469–496, https://doi.org/10.1146/annurev.fluid.35.101101.161147.

Brune, W. H., and Coauthors, 2016: Ozone production chemistry in the presence of urban plumes. *Faraday Discuss.*, **189**, 169–189, https://doi.org/10.1039/C5FD00204D.

Brunetti, M., G. Lentini, M. Maugeri, T. Nanni, I. Auer, R. Boehm, and W. Schoener, 2009: Climate variability and change in the greater Alpine region over the last two centuries based on multi-variable analysis. *Int. J. Climatol.*, **29**, 2197–2225, https://doi.org/10.1002/joc.1857.

Calfapietra, C., S. Fares, F. Manes, A. Morani, G. Sgrigna, and F. Loreto, 2013: Role of biogenic volatile organic compounds (BVOC) emitted by urban trees on ozone concentration in cities: A review. *Environ. Pollut.*, **183**, 71–80, https://doi.org/10.1016/j.envpol.2013.03.012.

Carpenter, L. J., K. C. Clemitshaw, R. A. Burgess, S. A. Penkett, J. N. Cape, and G. G. Mcfadyen, 1998: Investigation and evaluation of the NO_x/O_3 photochemical steady state. *Atmos. Environ.*, **32**, 3353–3365, https://doi.org/10.1016/S1352-2310(97)00416-0.

Carslaw, D. C., and G. Rhys-Tyler, 2013: New insights from comprehensive on-road measurements of NO_x, NO_2 and NH_3 from vehicle emission remote sensing in London, UK. *Atmos. Environ.*, **81**, 339–347, https://doi.org/10.1016/j.atmosenv.2013.09.026.

——, T. P. Murrells, J. Andersson, and M. Keenan, 2016: Have vehicle emissions of primary NO_2 peaked? *Faraday Discuss.*, **189**, 439–454, https://doi.org/10.1039/C5FD00162E.

Chemspider, 2018: Chemspider: Search and share chemistry. Accessed 31 July 2018, www.chemspider.com/.

Christen, A., and R. Vogt, 2004: Energy and radiation balance of a central European city. *Int. J. Climatol.*, **24**, 1395–1421, https://doi.org/10.1002/joc.1074.

——, M. W. Rotach, and R. Vogt, 2009: The budget of turbulent kinetic energy in the urban roughness sublayer. *Bound.-Layer Meteor.*, **131**, 193–222, https://doi.org/10.1007/s10546-009-9359-5.

Coggon, M. M., and Coauthors, 2016: Emissions of nitrogen-containing organic compounds from the burning of herbaceous and arboraceous biomass: Fuel composition dependence and the variability of commonly used nitrile tracers. *Geophys. Res. Lett.*, **43**, 9903–9912, https://doi.org/10.1002/2016GL070562.

Darbieu, C., and Coauthors, 2015: Turbulence vertical structure of the boundary layer during the afternoon transition. *Atmos. Chem. Phys.*, **15**, 10 071–10 086, https://doi.org/10.5194/acp-15-10071-2015.

De Arellano, J. V.-G., P. G. Duynkerke, and P. J. H. Builtjes, 1993: The divergence of the turbulent diffusion flux in the surface layer due to chemical reactions: The NO-O_3-NO_2 system. *Tellus*, **45B**, 23–33, https://doi.org/10.3402/tellusb.v45i1.15576.

De Gouw, J., C. Warneke, T. Karl, G. Eerdekens, C. Van der Veen, and R. Fall, 2003: Sensitivity and specificity of atmospheric trace gas detection by proton-transfer-reaction mass spectrometry. *Int. J. Mass Spectrom.*, **223–224**, 365–382, https://doi.org/10.1016/S1387-3806(02)00926-0.

Dolgorouky, C., and Coauthors, 2012: Total OH reactivity measurements in Paris during the 2010 MEGAPOLI winter campaign. *Atmos. Chem. Phys.*, **12**, 9593–9612, https://doi.org/10.5194/acp-12-9593-2012.

Dommen, J., A. S. H. Prevot, I. Polo, B. Neininger, and M. Baumle, 2001: Airborne NMHC measurements under various pollution conditions. *Int. J. Veh. Des.*, **27**, 217, https://doi.org/10.1504/IJVD.2001.001966.

Droste, A. M., G. J. Steeneveld, and A. A. M. Holtslag, 2018: Introducing the urban wind island effect. *Environ. Res. Lett.*, **13**, 094007, https://doi.org/10.1088/1748-9326/aad8ef.

Ehlers, C., D. Klemp, F. Rohrer, D. Mihelcic, R. Wegener, A. Kiendler-Scharr, and A. Wahner, 2016: Twenty years of ambient observations of nitrogen oxides and specified hydrocarbons in air masses dominated by traffic emissions in Germany. *Faraday Discuss.*, **189**, 407–437, https://doi.org/10.1039/C5FD00180C.

European Air Quality Agency, 2019: European Environment Agency. Accessed 1 October 2019, www.eea.europa.eu/.

Eurostat, 2019: Eurostat: Your key to European statistics. Accessed 1 October 2019, https://ec.europa.eu/eurostat/.

Franco, V., Posada Sanches, F., German, J., Mock, P., 2014: Real-world exhaust emissions from modern diesel cars. International Council on Clean Transportation Rep., 52 pp.

Fried, A., B. Henry, R. A. Ragazzi, M. Merrick, J. Stokes, T. Pyzdrowski, and R. Sams, 1992: Measurements of carbonyl sulfide in automotive emissions and an assessment of its importance to the global sulfur cycle. *J. Geophys. Res.*, **97**, 14 621–14 634, https://doi.org/10.1029/92JD01358.

Gimeno, T. E., and Coauthors, 2017: Bryophyte gas-exchange dynamics along varying hydration status reveal a significant carbonyl sulphide (COS) sink in the dark and COS source in the light. *New Phytol.*, **215**, 965–976, https://doi.org/10.1111/nph.14584.

Gkatzelis, G. I., and Coauthors, 2018: Gas-to-particle partitioning of major biogenic oxidation products: A study on freshly formed and aged biogenic SOA. *Atmos. Chem. Phys.*, **18**, 12 969–12 989, https://doi.org/10.5194/acp-18-12969-2018.

Gobiet, A., S. Kotlarski, M. Beniston, G. Heinrich, J. Rajczak, and M. Stoffel, 2014: 21st century climate change in the European Alps—A review. *Sci. Total Environ.*, **493**, 1138–1151, https://doi.org/10.1016/j.scitotenv.2013.07.050.

Goger, B., M. W. Rotach, A. Gohm, O. Fuhrer, I. Stiperski, and A. A. M. Holtslag, 2018: The impact of three-dimensional effects on the simulation of turbulence kinetic energy in a major Alpine valley. *Bound.-Layer Meteor.*, **168**, 1–27, https://doi.org/10.1007/s10546-018-0341-y.

Gohm, A., and Coauthors, 2009: Air pollution transport in an Alpine valley: Results from airborne and ground-based observations. *Bound.-Layer Meteor.*, **131**, 441–463, https://doi.org/10.1007/s10546-009-9371-9.

Grange, S. K., A. C. Lewis, S. J. Moller, and D. C. Carslaw, 2017: Lower vehicular primary emissions of NO_2 in Europe than assumed in policy projections. *Nat. Geosci.*, **10**, 914–918, https://doi.org/10.1038/s41561-017-0009-0.

Graus, M., M. Müller, and A. Hansel, 2010: High resolution PTR-TOF: Quantification and formula confirmation of VOC in real time. *J. Amer. Soc. Mass Spectrom.*, **21**, 1037–1044, https://doi.org/10.1016/j.jasms.2010.02.006.

Griffin, R. J., P. J. Beckman, R. W. Talbot, B. C. Sive, and R. K. Varner, 2007: Deviations from ozone photostationary state during the International Consortium for Atmospheric Research on Transport and Transformation 2004 campaign: Use of measurements and photochemical modeling to assess potential causes. *J. Geophys. Res.*, **112**, D10S07, https://doi.org/10.1029/2006JD007604.

Grimmond, C. S. B., and T. R. Oke, 1999: Aerodynamic properties of urban areas derived from analysis of surface form. *J. Appl. Meteor.*, **38**, 1262–1292, https://doi.org/10.1175/1520-0450(1999)038<1262:APOUAD>2.0.CO;2.

Grimmond, S., 2007: Urbanization and global environmental change: Local effects of urban warming. *Geogr. J.*, **173**, 83–88, https://doi.org/10.1111/j.1475-4959.2007.232_3.x.

Hellen, H., 2003: Determination of source contributions of NMHCs in Helsinki (60°N, 25°E) using chemical mass balance and the Unmix multivariate receptor models. *Atmos. Environ.*, **37**, 1413–1424, https://doi.org/10.1016/S1352-2310(02)01049-X.

Hodzic, A., P. S. Kasibhatla, D. S. Jo, C. D. Cappa, J. L. Jimenez, S. Madronich, and R. J. Park, 2016: Rethinking the global secondary organic aerosol (SOA) budget: Stronger production, faster removal, shorter lifetime. *Atmos. Chem. Phys.*, **16**, 7917–7941, https://doi.org/10.5194/acp-16-7917-2016.

Holzinger, R., A. Jordan, A. Hansel, and W. Lindinger, 2001: Methanol measurements in the lower troposphere near Innsbruck (047°16′N; 011°24′E), Austria. *Atmos. Environ.*, **35**, 2525–2532, https://doi.org/10.1016/S1352-2310(00)00430-1.

Jenkin, M. E., S. M. Saunders, and M. J. Pilling, 1997: The tropospheric degradation of volatile organic compounds: A protocol for mechanism development. *Atmos. Environ.*, **31**, 81–104, https://doi.org/10.1016/S1352-2310(96)00105-7.

Jimenez, J. L., and Coauthors, 2009: Evolution of organic aerosols in the atmosphere. *Science*, **326**, 1525–1529, https://doi.org/10.1126/science.1180353.

Karl, T., E. Apell, A. Hodzic, D. D. Riemer, D. R. Blake, and C. Wiedinmyer, 2009: Emissions of volatile organic compounds inferred from airborne flux measurements over a megacity. *Atmos. Chem. Phys.*, **9**, 271–285, https://doi.org/10.5194/acp-9-271-2009.

——, A. Hansel, L. Cappellin, L. Kaser, I. Herdlinger-Blatt, and W. Jud, 2012: Selective measurements of isoprene and 2-methyl-3-buten-2-ol based on NO_+ ionization mass spectrometry. *Atmos. Chem. Phys.*, **12**, 11 877–11 884, https://doi.org/10.5194/acp-12-11877-2012.

——, and Coauthors, 2017: Urban eddy covariance measurements reveal significant missing NO_x emissions in central Europe. *Sci. Rep.*, **7**, 2536, https://doi.org/10.1038/s41598-017-02699-9.

——, M. Striednig, M. Graus, A. Hammerle, and G. Wohlfahrt, 2018: Urban flux measurements reveal a large pool of oxygenated volatile organic compound emissions. *Proc. Natl. Acad. Sci. USA*, **115**, 1186–1191, https://doi.org/10.1073/pnas.1714715115.

Khalil, M. A. K., 2018: Steady states and transport processes in urban ozone balances. *npj Climate Atmos. Sci.*, **1**, 22, https://doi.org/10.1038/S41612-018-0035-7.

Kitz, F., K. Gerdel, A. Hammerle, T. Laterza, F. M. Spielmann, and G. Wohlfahrt, 2017: In situ soil COS exchange of a temperate mountain grassland under simulated drought. *Oecologia*, **183**, 851–860, https://doi.org/10.1007/s00442-016-3805-0.

Kljun, N., P. Calanca, M. W. Rotach, and H. P. Schmid, 2015: A simple two-dimensional parameterisation for flux footprint prediction (FFP). *Geosci. Model Dev.*, **8**, 3695–3713, https://doi.org/10.5194/gmd-8-3695-2015.

Kooijmans, L. M. J., and Coauthors, 2017: Canopy uptake dominates nighttime carbonyl sulfide fluxes in a boreal forest. *Atmos. Chem. Phys.*, **17**, 11 453–11 465, https://doi.org/10.5194/acp-17-11453-2017.

Kotthaus, S., and C. S. B. Grimmond, 2014: Energy exchange in a dense urban environment—Part I: Temporal variability of long-term observations in central London. *Urban Climate*, **10**, 261–280, https://doi.org/10.1016/j.uclim.2013.10.002.

Langford, B., B. Davison, E. Nemitz, and C. N. Hewitt, 2009: Mixing ratios and eddy covariance flux measurements of volatile organic compounds from an urban canopy (Manchester, UK). *Atmos. Chem. Phys.*, **9**, 1971–1987, https://doi.org/10.5194/acp-9-1971-2009.

Laughner, J. L., and R. C. Cohen, 2019: Direct observation of changing NO_x lifetime in North American cities. *Science*, **366**, 723–727, https://doi.org/10.1126/science.aax6832.

Lee, C.-L., and P. Brimblecombe, 2016: Anthropogenic contributions to global carbonyl sulfide, carbon disulfide and organosulfides fluxes. *Earth-Sci. Rev.*, **160**, 1–18, https://doi.org/10.1016/j.earscirev.2016.06.005.

Lee, J. D., and Coauthors, 2015: Measurement of NO_x fluxes from a tall tower in central London, UK and comparison with emissions inventories. *Environ. Sci. Technol.*, **49**, 1025–1034, https://doi.org/10.1021/es5049072.

Lehner, M., M. W. Rotach, and F. Obleitner, 2019: A method to identify synoptically undisturbed, clear-sky conditions for valley-wind analysis. *Bound.-Layer Meteor.*, **173**, 435–450, https://doi.org/10.1007/s10546-019-00471-2.

Leighton, P., 1961: *Photochemistry of Air Pollution*. 1st ed. E. M. Loebl, Ed., Academic Press, 300 pp.

Lenschow, D. H., A. C. Delany, B. B. Stankov, and D. H. Stedman, 1980: Airborne measurements of the vertical flux of ozone in the boundary layer. *Bound.-Layer Meteor.*, **19**, 249–265, https://doi.org/10.1007/BF00117223.

——, D. Gurarie, and E. G. Patton, 2016: Modeling the diurnal cycle of conserved and reactive species in the convective boundary layer using SOMCRUS. *Geosci. Model Dev.*, **9**, 979–996, https://doi.org/10.5194/gmd-9-979-2016.

Lindinger, W., and A. Jordan, 1998: Proton-transfer-reaction mass spectrometry (PTR-MS): On-line monitoring of volatile organic compounds at pptv levels. *Chem. Soc. Rev.*, **27**, 347–375, https://doi.org/10.1039/a827347z.

Llusia, J., J. Peñuelas, A. Guenther, and F. Rapparini, 2013: Seasonal variations in terpene emission factors of dominant species in four ecosystems in NE Spain. *Atmos. Environ.*, **70**, 149–158, https://doi.org/10.1016/j.atmosenv.2013.01.005.

Louka, P., S. E. Belcher, and R. G. Harrison, 2000: Coupling between air flow in streets and the well-developed boundary layer aloft. *Atmos. Environ.*, **34**, 2613–2621, https://doi.org/10.1016/S1352-2310(99)00477-X.

Mannschreck, K., S. Gilge, C. Plass-Duelmer, W. Fricke, and H. Berresheim, 2004: Assessment of the applicability of NO-NO_2-O_3 photostationary state to long-term measurements at the Hohenpeissenberg GAW Station, Germany. *Atmos. Chem. Phys.*, **4**, 1265–1277, https://doi.org/10.5194/acp-4-1265-2004.

McDonald, B. C., D. R. Gentner, A. H. Goldstein, and R. A. Harley, 2013: Long-term trends in motor vehicle emissions in U.S. urban areas. *Environ. Sci. Technol.*, **47**, 10 022–10 031, https://doi.org/10.1021/es401034z.

——, and Coauthors, 2018: Volatile chemical products emerging as largest petrochemical source of urban organic emissions. *Science*, **359**, 760–764, https://doi.org/10.1126/science.aaq0524.

National Academy of Sciences, 2016: *The Future of Atmospheric Chemistry Research: Remembering Yesterday, Understanding Today, Anticipating Tomorrow*. National Academies Press, 226 pp.

National Institute for Standards, 2018: NIST Chemistry WebBook, SRD 69. Accessed 31 July 2018, webbook.nist.gov/chemistry/form-ser/.

Nemitz, E., J. L. Jimenez, J. A. Huffman, I. M. Ulbrich, M. R. Canagaratna, D. R. Worsnop, and A. B. Guenther, 2008: An eddy-covariance system for the measurement of surface/atmosphere exchange fluxes of submicron aerosol chemical species—First application above an urban area. *Aerosol Sci. Technol.*, **42**, 636–657, https://doi.org/10.1080/02786820802227352.

Onida, M., 2019: Permanent Secretariat of the Alpine Convention: Activity Report 2017-2019. Alpine Convention Rep., 22 pp.

Prévôt, A. S. H., J. Dommen, M. Bäumle, and M. Furger, 2000: Diurnal variations of volatile organic compounds and local circulation systems in an Alpine valley. *Atmos. Environ.*, **34**, 1413–1423, https://doi.org/10.1016/S1352-2310(99)00440-9.

Rantala, P., and Coauthors, 2016: Anthropogenic and biogenic influence on VOC fluxes at an urban background site in Helsinki, Finland. *Atmos. Chem. Phys.*, **16**, 7981–8007, https://doi.org/10.5194/acp-16-7981-2016.

Reuter, M., and Coauthors, 2014: Decreasing emissions of NO_x relative to CO_2 in East Asia inferred from satellite observations. *Nat. Geosci.*, **7**, 792–795, https://doi.org/10.1038/ngeo2257.

Rotach, M. W., S.-E. Gryning, E. Batchvarova, A. Christen, and R. Vogt, 2004: Pollutant dispersion close to an urban surface? The BUBBLE tracer experiment. *Meteor. Atmos. Phys.*, **87**, 39–56, https://doi.org/10.1007/s00703-003-0060-9.

——, and Coauthors, 2005: BUBBLE—An urban boundary layer meteorology project. *Theor. Appl. Climatol.*, **81**, 231–261, https://doi.org/10.1007/s00704-004-0117-9.

——, and Coauthors, 2017: Investigating exchange processes over complex topography: The Innsbruck Box (i-Box). *Bull. Amer. Meteor. Soc.*, **98**, 787–805, https://doi.org/10.1175/BAMS-D-15-00246.1.

Sailor, D. J., 2014: Risks of summertime extreme thermal conditions in buildings as a result of climate change and exacerbation of urban heat islands. *Build. Environ.*, **78**, 81–88, https://doi.org/10.1016/j.buildenv.2014.04.012.

Schnitzhofer, R., J. Beauchamp, J. Dunkl, A. Wisthaler, A. Weber, and A. Hansel, 2008: Long-term measurements of CO, NO, NO_2, benzene, toluene and PM_{10} at a motorway location in an Austrian valley. *Atmos. Environ.*, **42**, 1012–1024, https://doi.org/10.1016/j.atmosenv.2007.10.004.

——, and Coauthors, 2009: A multimethodological approach to study the spatial distribution of air pollution in an Alpine valley during wintertime. *Atmos. Chem. Phys.*, **9**, 3385–3396, https://doi.org/10.5194/acp-9-3385-2009.

Schnitzler, J.-P., and Coauthors, 2002: Emission of biogenic volatile organic compounds: An overview of field, laboratory and modelling studies performed during the Tropospheric Research Program (TFS) 1997–2000. *J. Atmos. Chem.*, **42**, 159–177, https://doi.org/10.1023/A:1015757129946.

Schroeder, P., C. A. Belis, J. Schnelle-Kreis, R. Herzig, A. S. H. Prevot, M. Raveton, M. Kirchner, and M. Catinon, 2013: Why air quality in the Alps remains a matter of concern. The impact of organic pollutants in the alpine area. *Environ. Sci. Pollut. Res.*, **21**, 252–267, https://doi.org/10.1007/s11356-013-2058-2.

Seibert, P., H. Feldmann, B. Neininger, M. Bäumle, and T. Trickl, 2000: South foehn and ozone in the eastern Alps—Case study and climatological aspects. *Atmos. Environ.*, **34**, 1379–1394, https://doi.org/10.1016/S1352-2310(99)00439-2.

Simpson, D., and Coauthors, 1999: Inventorying emissions from nature in Europe. *J. Geophys. Res.*, **104**, 8113–8152, https://doi.org/10.1029/98JD02747.

Sinha, V., and Coauthors, 2012: Constraints on instantaneous ozone production rates and regimes during DOMINO derived using in-situ OH reactivity measurements. *Atmos. Chem. Phys.*, **12**, 7269–7283, https://doi.org/10.5194/acp-12-7269-2012.

Spielmann, F. M., and Coauthors, 2019: Gross primary productivity of four European ecosystems constrained by joint CO_2 and COS flux measurements. *Geophys. Res. Lett.*, **46**, 5284–5293, https://doi.org/10.1029/2019GL082006.

Statistik Austria, 2019: Statistik Austria: Die informationsmanager. Accessed 1 October 2019, www.statistik.at/.

Stimler, K., D. Nelson, and D. Yakir, 2010: High precision measurements of atmospheric concentrations and plant exchange rates of carbonyl sulfide using mid-IR quantum cascade laser. *Global Change Biol.*, **16**, 2496–2503, https://doi.org/10.1111/j.1365-2486.2009.02088.x.

Stolzenburg, D., and Coauthors, 2018: Rapid growth of organic aerosol nanoparticles over a wide tropospheric temperature range. *Proc. Natl. Acad. Sci. USA*, **115**, 9122–9127, https://doi.org/10.1073/pnas.1807604115.

Sulzer, P., and Coauthors, 2013: Applications of switching reagent ions in proton transfer reaction mass spectrometric instruments for the improved selectivity of explosive compounds. *Int. J. Mass Spectrom.*, **354–355**, 123–128, https://doi.org/10.1016/j.ijms.2013.05.004.

Tan, J., and Coauthors, 2009: The urban heat island and its impact on heat waves and human health in Shanghai. *Int. J. Biometeor.*, **54**, 75–84, https://doi.org/10.1007/s00484-009-0256-x.

Theeuwes, N. E., G.-J. Steeneveld, R. J. Ronda, M. W. Rotach, and A. A. M. Holtslag, 2015: Cool city mornings by urban heat. *Environ. Res. Lett.*, **10**, 114022, https://doi.org/10.1088/1748-9326/10/11/114022.

Umweltbundesamt Austria, 2019: Umweltbundesamt: Perspektiven für umwelt und gesellschaft. Accessed 15 August 2019, www.umweltbundesamt.at/.

United Nations, 2019: United Nations Department of Economic and Social Affairs: Population dynamics. Accessed 1 October 2019, https://population.un.org/wpp/.

US EPA, 2017: Estimation Programs Interface Suite™ for Microsoft® Windows 10, Version 1903. United States Environmental Protection Agency.

Vaughan, A. R., and Coauthors, 2017: VOC emission rates over London and south east England obtained by airborne eddy covariance. *Faraday Discuss.*, **200**, 599–620, https://doi.org/10.1039/C7FD00002B.

Velasco, E., and Coauthors, 2009: Eddy covariance flux measurements of pollutant gases in urban Mexico City. *Atmos. Chem. Phys.*, **9**, 7325–7342, https://doi.org/10.5194/acp-9-7325-2009.

Vergeiner, I., and E. Dreiseitl, 1987: Valley winds and slope winds? Observations and elementary thoughts. *Meteor. Atmos. Phys.*, **36**, 264–286, https://doi.org/10.1007/BF01045154.

Vinuesa, J. F., and J. V. G. De Arellano, 2003: Fluxes and (co-)variances of reacting scalars in the convective boundary layer. *Tellus*, **55B**, 935–949, https://doi.org/10.3402/TELLUSB.V55i4.16382.

Vogt, R., A. Christen, M. W. Rotach, M. Roth, and A. N. V. Satyanarayana, 2005: Temporal dynamics of CO_2 fluxes and profiles over a central European city. *Theor. Appl. Climatol.*, **84**, 117–126, https://doi.org/10.1007/s00704-005-0149-9.

Whelan, M. E., and Coauthors, 2018: Reviews and syntheses: Carbonyl sulfide as a multi-scale tracer for carbon and water cycles. *Biogeosciences*, **15**, 3625–3657, https://doi.org/10.5194/bg-15-3625-2018.

Zängl, G., 2004: A reexamination of the valley wind system in the Alpine Inn Valley with numerical simulations. *Meteor. Atmos. Phys.*, **87**, 241–256, https://doi.org/10.1007/s00703-003-0056-5.

Zentralanstalt für Meteorologie und Geophysik, 2018: Welcome to HISTALP! Accessed 31 December 2018, www.zamg.ac.at/histalp/.

Zhang, H., and Coauthors, 2018: Monoterpenes are the largest source of summertime organic aerosol in the southeastern United States. *Proc. Natl. Acad. Sci. USA*, **115**, 2038–2043, https://doi.org/10.1073/pnas.1717513115.

Zhang, Y., and Coauthors, 2016: Large vertical gradient of reactive nitrogen oxides in the boundary layer: Modeling analysis of DISCOVER-AQ 2011 observations. *J. Geophys. Res.*, **121**, 1922–1934, https://doi.org/10.1002/2015JD024203.

Zumkehr, A., T. W. Hilton, M. Whelan, S. Smith, L. Kuai, J. Worden, and J. E. Campbell, 2018: Global gridded anthropogenic emissions inventory of carbonyl sulfide. *Atmos. Environ.*, **183**, 11–19, https://doi.org/10.1016/j.atmosenv.2018.03.063.